

SAM3D: Segment Anything Model in Volumetric Medical Images

Nhat-Tan Bui^{1*}, Dinh-Hieu Hoang^{2-4*}, Minh-Triet Tran²⁻⁴, Ngan Le¹

¹University of Arkansas, Fayetteville, Arkansas, USA

²University of Science, VNU-HCM

³John von Neumann Institute, VNU-HCM

⁴Vietnam National University, Ho Chi Minh City, Vietnam

tanb@uark.edu, hieu.hoang2020@ict.jvn.edu.vn, tmtriet@hcmus.edu.vn, thile@uark.edu

Abstract

Image segmentation is a critical task in medical image analysis, providing valuable information that helps to make an accurate diagnosis. In recent years, deep learning-based automatic image segmentation methods have achieved outstanding results in medical images. In this paper, inspired by the Segment Anything Model (SAM), a foundation model that has received much attention for its impressive accuracy and powerful generalization ability in 2D still image segmentation, we propose a SAM3D that targets at 3D volumetric medical images and utilizes the pre-trained features from the SAM encoder to capture meaningful representations of input images. Different from other existing SAM-based volumetric segmentation methods that perform the segmentation by dividing the volume into a set of 2D slices, our model takes the whole 3D volume image as input and processes it simply and effectively that avoids training a significant number of parameters. Extensive experiments are conducted on multiple medical image datasets to demonstrate that our network attains competitive results compared with other state-of-the-art methods in 3D medical segmentation tasks while being significantly efficient in terms of parameters.

1. Introduction

Volumetric segmentation is one of the most essential tasks in medical image analysis, having numerous applications in diagnosing pathologies, surgical planning, research, and computer-aided diagnosis. Volumetric medical images, such as computed tomography (CT), magnetic resonance imaging (MRI), optical coherence tomography (OCT), and digital breast tomosynthesis (DBT), consist of a sequence of two-dimensional (2D) images arranged in a stack, which provides a precise portrayal of the body's three-dimensional

(3D) anatomical structures [29]. In dealing with this kind of image, segmentation is used to identify and isolate specific regions of interest, such as abnormalities and pathologies, and make it easier for radiologists to better understand and interpret the data.

With the development of deep learning (DL), many approaches have gained prominent performance in 3D medical segmentation, pioneered by UNet [23] and its variations. Despite gaining promising results, CNN-based methods struggled to make breakthroughs due to the limitation of the convolution receptive field. Recently, Vision Transformer (ViT) [7] and other transformer-based works like Swin-UNet [4] have revealed the potential of the self-attention mechanism in capturing long-range relationships in visual data that performs well at both classification and dense prediction tasks. It is widely believed that the features extracted by transformer blocks are innately global since every single patch interacts with all other patches impartially, regardless of their locations. Therefore, integrating CNNs and transformers to extract both low-level features and semantic information is an appealing approach to building strong and robust models. Currently, several works have been taking this hybrid approach, such as TransUNet [5], UNETR [9], and MISSFormer [13], and obtaining promising results.

However, since the primary focus of these works is to enhance segmentation accuracy, this often increases the model complexity in terms of parameters and ad-hoc hypotheses. As a consequence, the models consist of sophisticated modules containing an enormous number of parameters that it may take up to weeks to be trained with low-cost hardware configurations as well as their task-specific architectures make them prone to perform poorly when taken into other scenarios. To reduce training costs, leverage auxiliary data, and avoid using complicated techniques, it is plausible to take advantage of pre-trained models by using them to initialize model parameters or as feature extractors. Furthermore, recently, a series of foundation mod-

*Equal contribution

els trained on Internet-scale datasets have been introduced [6, 22, 26, 28]. Remarkably, SAM [17] is a powerful promptable transformer-based foundation model for image segmentation, which is trained on SA-1B dataset, including more than 1 billion masks and millions of natural images. This foundation model has powerful generalization ability, performing very well on several general downstream segmentation tasks. This motivates us to find an appropriate approach to build robust SAM-based models for medical image segmentation.

In this work, we propose a simple yet efficient architecture for the volumetric medical segmentation task, named SAM3D, which is built upon the SAM’s encoder with a simple 3D CNN decoder. In particular, we freeze the SAM’s encoder and leverage it as the feature extractor to generate meaningful features for the input volume. Distinct from previous SAM-based methods predicting slide by slide, we divide the 3D input volume along the depth dimension, and then the SAM’s encoder takes each slice as input to produce the feature maps. All the feature maps are then concatenated along the depth dimension and put into our simple 3D decoder to generate the final result. This simple strategy surprisingly attains competitive results compared with other state-of-the-art 3D models. To the best of our knowledge, our method is the first to apply SAM in a 3D volume manner to segment medical images. To sum up, our contributions can be summarized as follows:

- We propose adapting SAM for the 3D volume. We believe this simple strategy can be further extended with ease, and used in other 3D domains, not just for medical images.
- We implement SAM3D, a 3D segmentation model for medical images based on SAM, with a simple 3D CNN decoder. Our method leverages the power of SAM for 3D medical images to alleviate the problem of huge parameters of the existing methods and target the weak boundary problem.
- We demonstrate the effectiveness of our method by conducting experiments with SAM3D on three datasets, including ACDC [2], Synapse [18], MSD BraTS [25] and MSD Lung [25].

2. Related Work

The emergence of UNet [23] has brought about a new era for deep learning in medical image analysis. The U-shaped architecture has become a fundamental design for most state-of-the-art methods [3, 15, 21, 32] in medical image segmentation. Later, after ViT [7] showed the power of the Transformer-based self-attention mechanism [27] in image classification, several works have explored the potential of Transformer to leverage the long-range dependencies

and global feature representations for visual data. Recently, the rise of foundation models trained on Internet-scale natural image datasets has sparked the idea of exploiting these models in medical image segmentation. In this section, we first review the current methodologies, which focus on designing architectures that combine the merit of CNN and Transformer. Then we introduce SAM, a foundation model for segmenting natural images, and some recent works using SAM in the medical image field.

Segmentation Methods based on CNN and Transformer: In the beginning, the works that sparked the trend of leveraging Transformer in medical images try to integrate Transformer blocks into a U-shaped CNN. TransUNet [5] successfully merges CNN and Transformer into one framework to capture both localized spatial and global information. The network, which follows U-shaped architecture, first utilizes CNN for feature extraction and then applies additional Transformer layers to the convolution features to fortify the features with long-range relationships. Swin-Unet [4] replaces all convolutional blocks in U-Net by Swin Transformer [19] blocks to construct a pure Transformer-based U-shaped architecture. nnUNet [14] proposes the self-adapting framework for both 2D and 3D medical segmentation. MISSFormer [13] proposes the Enhanced Transformer Block to extract better the hierarchical feature representation containing both long-range dependencies and local information with low computational cost. After that, all obtained features at different stages are passed through the Enhanced Transformer Context Bridge to achieve multi-scale information aggregation. TransDeepLab [1] is another work that incorporates Swin Transformer blocks with Atrous Spatial Pyramid Pooling (ASPP) module and proposes cross-contextual attention to attain and fuse multi-scale information. HiFormer [11] introduces the Double-Level Fusion (DLF) module for fusing the coarse and fine-grained feature representations. UNETR [9] adopts Transformer to directly encode 3D input patches and combines the feature extraction with the CNN-based decoder at multiple resolutions. Later, Swin UNETR [8] leverages the Swin Transformer block in the encoder to enhance the performance of UNETR. nnFormer [31] combines CNN and Transformer block in an interleaved fashion with the feature pyramids to fully capture and blend local and global information. UNETR++ [24] introduces the efficient paired-attention (EPA) module into the previous UNETR framework to better learn the spatial-channel feature information.

Segment Anything Model: Foundation models [6, 22, 26, 28], or so-called base models, are machine learning models trained on very large-scale datasets (Internet-scale, or web-scale in some contexts) such that they can be used in many related downstream tasks without too many modifications. As far as we know, the Segment Anything Model

(SAM) [17] is the first foundation model for natural image segmentation that users can guide the segmentation with prompt engineering. The model consists of three components, image encoder, prompt encoder, and lightweight mask decoder, and is trained on promptable segmentation tasks to achieve generalization. Instead of relying completely on data on the Internet, the authors train SAM with model-in-the-loop annotation strategy and produce SA-1B dataset which includes 11 million images and 1 billion corresponding masks. The remarkable performance of SAM on many types of promptable natural image segmentation tasks draws researchers’ attention to answering the question of whether we can apply SAM in some way to segment images from other domains, like medical images. SAMed [30] adapts SAM into the medical image domain by using a reparametrization method called the Low-Rank Adaptation (LoRA) [12] on image encoder along with many other techniques like warmup finetuning and AdamW optimizer to adjust prompt encoder and mask decoder. This model gains competitive results on the Synapse multi-organ segmentation dataset, proving the powerful generalization of SAM is still useful in such an extremely different domain. Another work, MedSAM [20] aims to create a foundation model for the medical image domain by re-training SAM on a union of several medical image datasets with over 1 million images in total, across many imaging protocols and modalities.

The aforementioned works depend on the idea of finetuning SAM, splitting 3D images into 2D slices as input data, and stacking multiple 2D predictions to form the final 3D prediction. Although attaining promising results, these strategies neglect depth-wise information, which deters the model’s awareness of anatomical structures and global information. Additionally, developing methods for a particular dataset is no longer practical due to the limited scope of generalization. From the above analysis, as a consequence, we propose a volumetric segmentation approach that utilizes the strength of SAM to ameliorate the performance of 3D medical segmentation and avoid designing large models and slice-by-slice predicted fashion.

3. Method

In this section, we will introduce our model, termed SAM3D, as well as explain the reasoning behind this simple design. In short, our goal is to design a simple adaptation of SAM such that the model should take advantage of SAM without having to re-train too many parameters or construct too complicated and task-specific modules.

3.1. Overall Architecture

SAM owns a powerful image encoder that can extract meaningful feature representations for natural images. Unfortunately, when it comes to 3D medical images, we ob-

serve that the difference between the two domains makes it inappropriate to hope that the original SAM image encoder can extract the true semantic information of the medical images. However, we hypothesize that the feature representation from the SAM image encoder is not completely useless. It contains both high-level features, which are meaningless in the medical image domain, and low-level features including edges, boundaries, blobs, regions, etc. which are still valuable in every image domain. As a consequence, we find it tempting to keep the SAM image encoder unchanged and just use another decoder so that we are able to minimize the number of parameters that need to be trained.

Unlike SAMed and MedSAM [20, 30], instead of finetuning all 3 components of SAM, our method leverages the original SAM’s image encoder as the feature extractor in a slice-by-slice fashion and a lightweight 3D image decoder, as depicted by in Figure 1. Specifically, the input has resolution $H \times W \times D$, split into D 2D slices which are triplicated into $H \times W \times 3$ with 3 identical channels so that it can be put through SAM’s image encoder. The feature maps extracted by the image encoder are stacked into a 3D feature map $H \times W \times D \times C$ where C is the number of channels. As SAM’s mask encoder is designed for 2D image segmentation, we decided to replace it with a 3D lightweight decoder. The 3D feature map is processed by this lightweight decoder to produce the final prediction. In this way, the depth-wise information is efficiently incorporated so that the decoder can learn more and exploit better the anatomical structures. We also observe different medical image modalities have their own distinct characteristics. As a result, using the prompt encoder may degrade the performance since it hinders the extracted feature from obtaining distinctive information that varies by modality. For that reason, we remove the prompt encoder and use a decoder with a simple classifier.

3.2. Encoder

As mentioned before, the feature extracted by SAM’s image encoder is supposed to have robust and valuable low-level information regardless of the image domain. Thus, it is plausible to tackle the notorious weak boundary in the medical image domain by using features extracted by SAM’s image encoder. Furthermore, although the difference between 3D medical images and 2D natural images is so large that it seems necessary to finetune the image encoder, any modification to the weights of the encoder might degrade the quality of the extracted low-level feature. Therefore, we freeze the image encoder and train a new lightweight decoder. In Section 4, we will show that this approach can utilize the information about the texture, intensity, contrast between regions, etc. to effectively construct semantic information specific to 3D medical images and thus yield precise segmentation results.

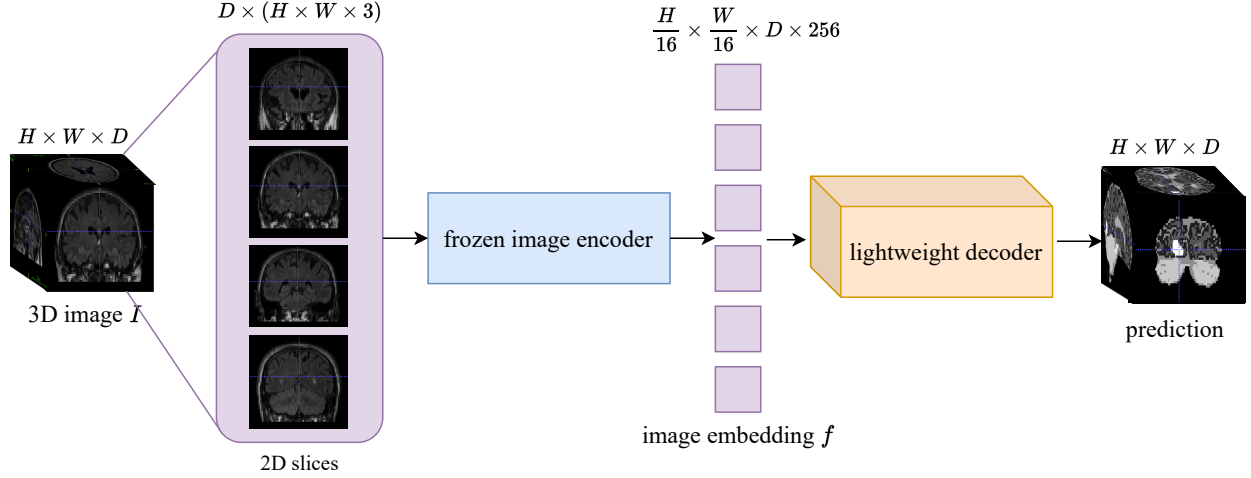


Figure 1. Overall architecture of the proposed SAM3D, including two modules, i.e., *2D image encoder*, which is derived from Segment Anything Model without any modification, and *3D lightweight decoder*, which utilizes 3D convolutional blocks to incorporate depth-wise information to infer the prediction. In this context, H , W , and D respectively represent the input height, width, and depth.

Formally, let $I \in \mathbb{R}^{H \times W \times D}$ be the input, and Enc denote the image encoder. First, I is split along the depth dimension into D slices. Each i -th slice is triplicated to have 3 identical channels, denoted by $I_i \in 3 \times H \times W$. Enc takes I_i as input and outputs corresponding slice embedding.

$$f_i = Enc(I_i), \text{ where } f_i \in \mathbb{R}^{\frac{H}{16} \times \frac{W}{16} \times D \times 256} \quad (1)$$

We stack these slice embeddings and transpose the result to obtain the final 3D image embedding.

$$f \in \mathbb{R}^{\frac{H}{16} \times \frac{W}{16} \times D \times 256} \quad (2)$$

3.3. Decoder

Because our decoder must have the ability to deal with 3D patches, we cannot take advantage of SAM’s mask decoder which is tailored to 2D natural images but choose another decoder and train it from scratch. Vision Transformer [7] and its variants are excluded due to its quadratic computational complexity in terms of the number of patches. It is notable that the number of patches is now D times greater than itself in 2D settings, where D is up to hundreds. Therefore, we decided to use a simple decoder having 4 3D convolutional blocks with skip connections [10] and a segmentation head, as illustrated in detail by Figure 2.

3.4. Objective Function

Following nnFormer [31], we utilize both dice loss and cross-entropy loss as loss functions to train our network. It is defined as follows:

$$\mathcal{L}(X, Y) = - \sum_{i=1}^I \left(\frac{2 \times \sum_{j=1}^J X_{j,i} Y_{j,i}}{\sum_{j=1}^J X_{j,i}^2 + \sum_{j=1}^J Y_{j,i}^2} + \sum_{j=1}^J X_{j,i} \log Y_{j,i} \right) \quad (3)$$

where, I is the number of classes, J denotes the number of voxels, $X_{j,i}$ and $Y_{j,i}$ denote the ground truths and predictions at voxel j for class i , respectively.

We also adopt the deep supervision technique for multiple decoding stages. Specifically, the output features of each decoding stage are passed through the segmentation block, including one $3 \times 3 \times 3$ and one $1 \times 1 \times 1$ convolution layer, to generate the prediction of one typical stage. To calculate the loss value at one typical stage, we down-sample the ground truth equal to the prediction resolution. Therefore, the final loss can be defined as follows:

$$\mathcal{L}_{total} = \sum_{i=1}^n \alpha_i \times \mathcal{L}_i \quad (4)$$

where n , which we set equal to 3, is the number of decoder layers. α_i denotes the hyper-parameter to control the contribution of different resolutions to the final loss function. In practice, $\alpha_2 = \frac{\alpha_1}{2}$ and $\alpha_3 = \frac{\alpha_1}{4}$ and all α hyper-parameters are normalized to 1.

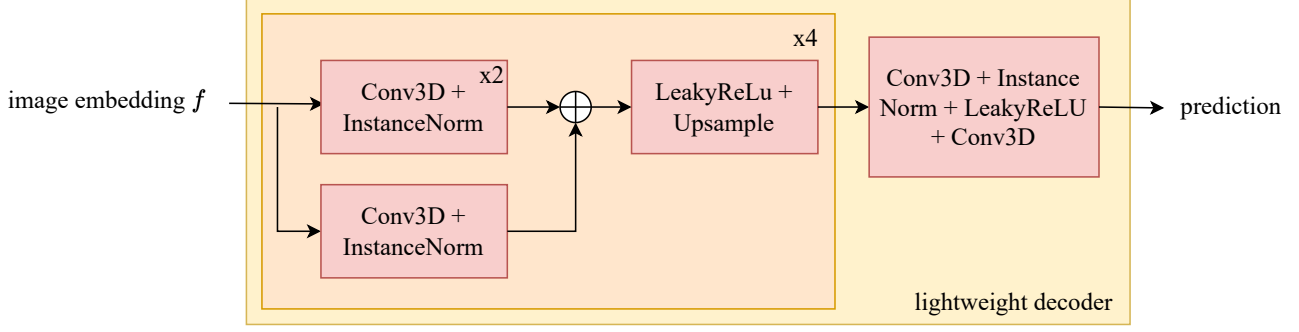


Figure 2. Architecture of the 3D lightweight decoder.

4. Experiments

4.1. Dataset

To validate the effectiveness of our model, we conduct the experiments on three datasets: Automated Cardiac Diagnosis (ACDC) [2], Multi-organ CT Segmentation (Synapse) [18], Brain Tumor Segmentation (BraTS) [25] and Lung Tumor Segmentation (Lung) [25]. BraTS and Lung come from the Medical Segmentation Decathlon challenge (MSD) [25]. For a fair comparison, we follow the data splitting of previous works. The details are conveyed below.

ACDC (MRI): The ACDC dataset includes cardiac MRI images of 100 patients, which come from five different groups: healthy, previous myocardial infarction with altered left ventricular ejection fraction, dilated cardiomyopathy, hypertrophic cardiomyopathy and abnormal right ventricle. The ground truth labels consist of the right ventricle (RV), left ventricle (LV) and myocardium (MYO). Following nnFormer [31] and UNETR++ [24], we split the dataset into 70 training samples, 10 validation samples and 20 test samples.

Synapse (CT): The Synapse dataset includes abdominal CT scans of 30 subjects, which are variable volume sizes from $512 \times 512 \times 85$ to $512 \times 512 \times 198$. The voxel dimension ranges from $0.54 \times 0.54 \text{ mm}^2$ to $0.98 \times 0.98 \text{ mm}^2$, and the thickness of the scanned slices varies from 2.5 mm to 5.0 mm. The ground truth labels consist of the spleen, right kidney, left kidney, gallbladder, esophagus, liver, stomach, aorta, inferior vena cava, portal vein and splenic vein, pancreas, right adrenal gland, and left adrenal gland. Some patients lack the right kidney or gallbladder, and therefore they are not labelled. Following nnFormer [31] and UNETR++ [24], we split the dataset into 18 training and 12 testing samples.

BraTS (MRI): The BraTS dataset includes 484 MRI scans, which is the subset of the 2016 and 2017 Brain Tumour Image Segmentation (BraTS) challenges. Each scan consists of four modalities: FLAIR, T1w, T1gd and T2w.

The voxel dimension is $1.0 \times 1.0 \times 1.0 \text{ mm}^3$. We evaluate the results of the whole tumor (WT), enhancing tumor (ET) and tumor core (TC). Following UNETR [9], nnFormer [31], we split 484 MRI images into 80:15:5 for training, validation and testing.

Lung (CT): The Lung dataset, which is public through TCIA¹, includes CT scans from 96 patients. The 3D volumes are taken with a section thickness of less than 1.5 mm, 120 kVp, automatic tube current modulation range of 100-700 mA, tube rotation speed of 0.5s, the helical pitch of 0.9-1.0, and a sharp reconstruction kernel. The goal of this dataset is to segment the small lung tumors from the large background; thus the ground truth labels consist of background and cancer. Following UNETR++ [24], we split 63 CT volumes into 8:2 for training and validation.

4.2. Evaluation Metrics

In order to compare the performance of our method with previous state-of-the-art models, we employ two metrics: Dice Similarity Coefficient (DSC) and 95% Hausdorff Distance (HD95).

Dice Similarity Coefficient (DSC): The Sørensen–Dice index or Dice coefficient measures the pixel-wise similarity between the volumetric prediction and ground truth segmentation mask. It is defined as follows:

$$\text{DSC}(X, Y) = \frac{2 \times |X \cap Y|}{|X| + |Y|} \quad (5)$$

where X is the ground truth, Y is the prediction, and \cap is the intersection operator. This metric is referred to as a regional measure that takes into consideration the overlapping region over the union region of the model’s predicted map and the ground truth.

95% Hausdorff Distance (HD95): The Hausdorff distance (HD) measures the longest distance of a point in one set to the closest point in the other set. HD is a useful distance in the segmentation task because it indicates the

¹<https://www.cancerimagingarchive.net/>

Table 1. Quantitative results on Synapse dataset. We report the mean DSC and mean HD95 on the spleen (Spl), right kidney (RKid), left kidney (LKid), gallbladder (Gal), liver (Liv), stomach (Sto), aorta (Aor) and pancreas (Pan). Note: The number of training parameters is counted in millions.

SAM-based	Approaches	Methods	Spl	RKid	LKid	Gal	Liv	Sto	Aor	Pan	HD↓	DSC↑	Params
✗	2D	TransUNet [5]	85.08	77.02	81.87	63.16	94.08	75.62	87.23	55.86	31.69	77.49	96.07
		Swin-Unet [4]	90.66	79.61	83.28	66.53	94.29	76.60	85.47	56.58	21.55	79.13	27.17
		TransDeepLab [1]	89.00	79.88	84.08	69.16	93.53	78.40	86.04	61.19	21.25	80.16	21.14
		HiFormer-S [11]	91.03	64.84	82.39	73.29	94.22	78.07	85.63	60.84	18.85	80.29	23.25
		HiFormer-B [11]	90.99	79.77	85.23	65.69	94.61	81.08	86.21	59.52	14.70	80.39	25.51
		HiFormer-L [11]	90.44	78.37	84.23	68.61	94.07	82.03	87.03	60.77	19.14	80.69	29.52
	3D	MISSFormer [13]	91.92	82.00	85.21	68.65	94.41	80.81	86.99	65.67	18.20	81.96	—
		nnFormer [31]	90.51	86.25	86.57	70.17	96.84	86.83	92.04	83.35	10.63	86.57	150.50
		UNETR [9]	85.00	84.52	85.60	56.30	94.57	70.46	89.80	60.47	18.59	78.35	92.49
✓	2D	SAMed [30]	88.72	79.95	80.45	69.11	94.80	82.06	87.77	72.17	20.64	81.88	18.81
		SAMed_s [30]	85.81	78.92	79.63	57.11	93.98	77.49	83.62	65.66	—	77.78	6.32
	3D	SAM3D	84.29	85.64	86.31	49.81	95.42	76.11	89.57	69.32	17.87	79.56	1.88

largest segmentation error in terms of the discrepancy between two boundaries [16]. 95% HD calculates the 95th percentile of the HD between boundaries of the volumetric prediction and ground truth segmentation mask.

$$\text{HD}(X, Y) = \max\{d_{XY}, d_{YX}\} \quad (6)$$

where d_{XY} is the greatest distance between the ground truth X and the prediction Y , and d_{YX} is the greatest distance between the prediction Y and the ground truth X .

4.3. Implementation Details

Our model is implemented based on Python 3.8.10 with PyTorch library and trained on a single NVIDIA RTX 2080 Ti GPU with 11GB memory. We integrate our model into the nnUNet [14] framework for fairness. We use **ViT-B** version as our backbone for the SAM’s image encoder due to the limited resources. instead of exhaustively finding an overfitting training procedure, we trained our model with the general training strategy of nnFormer [31] and UNETR++ [24], the stochastic gradient descent (SGD) with a momentum of 0.99 and a weight decay of $3e-5$. The learning rate scheduler is defined as $lr = \text{init_lr} \times (1 - \frac{\text{epoch}}{\text{max_epoch}})^{\text{power}}$, where $\text{init_lr} = 1e-2$, $\text{power} = 0.9$, and $\text{max_epoch} = 1000$. One epoch consists of 250 iterations. For ACDC, Synapse, BraTS, and Lung datasets, we train our model with the 3D volume sizes of $160 \times 160 \times 14$, $176 \times 176 \times 64$, $64 \times 64 \times 64$ and $192 \times 192 \times 34$, respectively. We also utilize the same data augmentation techniques for nnFormer, which are rotation, scaling, brightness adjustment, gamma augmentation, and mirroring. The batch size is set to 4 for ACDC and 2 for Synapse, BraTS, and Lung.

4.4. Performance Comparisons

We perform the experiments on four datasets by comparing our SAM3D with several previous state-of-the-art

Table 2. Quantitative results on ACDC dataset. We report the mean DSC metric on the right ventricle (RV), left ventricle (LV) and myocardium (MYO). Note: The number of training parameters is counted in millions.

Methods	RV	LV	MYO	Average	Params
TransUNet [5]	88.86	84.54	95.73	89.71	96.07
Swin-Unet [4]	88.55	85.62	95.83	90.00	27.17
UNETR [9]	85.29	86.52	94.02	86.61	92.49
MISSFormer [13]	86.36	85.75	91.59	87.90	—
nnFormer [31]	90.94	89.58	95.65	92.06	150.50
UNETR++ [24]	91.89	90.61	96.00	92.83	66.80
SAM3D	89.44	87.12	94.67	90.41	1.88

(SOTA) methods. All the performance results are excerpted from UNETR++ [24] and original papers when the results are available. Those SOTA methods include both 2D and 3D approaches, also SAM-based and non-SAM-based. Therefore, we believe those works are the most representative to compare to demonstrate the effectiveness of our method.

4.4.1 Model Complexity

We report the training parameters for each method in Table 1, Table 2, Table 3, and Table 4. In comparison, our SAM3D significantly reduces the number of trainable parameters compared with other methods. Since we freeze the SAM’s encoder, with only 1.88M trainable parameters from our decoder, our method still obtains comparable results with other previous SOTA. Note that for the dataset with more than one modality, the number of parameters needed for our first decoder block will be multiplied by the number of modalities. For instance, for the BraTS dataset, the number of trainable parameters of our model is 4.63M. But this number is still very small compared to nnFormer (150.50M) or UNETR++ on the Lung dataset (121.17M).

Table 3. Quantitative results on BraTS dataset. We report the mean DSC and mean HD95 on whole tumor (WT), enhancing tumor (ET), and tumor core (TC). The result of UNETR++ [24] is reported based on the official checkpoint. It is noteworthy that our model is trained with the image size of $64 \times 64 \times 64$, whereas nnFormer [31] and UNETR++ [24] are trained with the image size of $128 \times 128 \times 128$.

Methods	Average		WT		ET		TC		Params
	HD↓	DSC↑	HD↓	DSC↑	HD↓	DSC↑	HD↓	DSC↑	
TransUNet [5]	12.98	64.4	14.03	70.6	10.42	54.2	14.5	68.4	96.07
UNETR [9]	8.82	71.1	8.27	78.9	9.35	58.5	8.85	76.1	92.49
nnFormer [31]	4.05	86.4	3.80	91.3	3.87	81.8	4.49	86.0	150.50
UNETR++ [24]	5.85	77.7	4.79	91.2	4.22	78.5	6.78	78.4	42.65
SAM3D	8.72	72.9	6.03	88.0	10.05	69.6	9.79	76.6	4.63

4.4.2 Quantitative Comparison

Table 4. Quantitative results on Lung dataset. We report the mean DSC metric on the tumor cancer. Note: The number of training parameters is counted in millions.

Methods	DSC↑	Params
nnUNet [14]	74.31	—
Swin UNETR [8]	75.55	62.83
nnFormer [31]	77.95	150.50
UNETR [9]	73.29	92.49
UNETR++ [24]	80.68	121.17
SAM3D	71.42	1.88

We compared our SAM3D with recent state-of-the-art methods like TransUNet [5], UNETR [9], nnFormer [31]. Despite the fact that SAM3D cannot be counted as being outstanding from the compared methods, our approach achieves promising performance that is led by the currently best methods just narrow margins. This result implies that we can keep the SAM’s image encoder unchanged so that even an extremely simple, general-purpose, and lightweight 3D convolutional decoder can (1) remove the false semantic information stemming from the discrepancy between 3D medical images and 2D natural images, (2) reconstruct the true semantic information from the superior low-level features extracted by SAM’s encoder, and (3) fully take advantage of this local information to reconstruct the exact boundaries of objects of interest. Another intriguing thing is that the weak result of SAMed.s [30], where the LoRA finetuning technique is utilized for the decoder, compared to SAMed and our SAM3D indirectly proves the semantic information is prone to be fabricated if the decoder is not thoroughly retrained. Moreover, in spite of a simple and shallow decoder with a narrow receptive field, our model SAM3D still beats SAMed at HD95 metric. That proves the depth-wise information helps the decoder reconstruct the anatomical structures in a more accurate manner.

4.5. Ablation Study

We conducted the ablation study to demonstrate the effectiveness of the skip connections in our decoder, as shown in Tab. 5. It is apparent that the skip connections have a

positive effect, slightly improving the performance of the model. We think the skip connections help retain information about edges and boundaries so that the segmentation is more precisely performed.

5. Conclusion

In this work, we propose SAM3D, a simple model designed for 3D medical image segmentation. Our method leverages the power of SAM pre-trained encoder with our simple decoder to achieve competitive results in several 3D datasets. Since SAM has revolutionized the natural image segmentation task, we have been able to demonstrate its potential in medical image segmentation as well. We hope this research will inspire future researchers to advance the field of medical segmentation further.

Future Direction: In our experiment, we only utilize the smallest version of SAM, which is SAM.b, due to the limited resources and time. We believe that the SAM.l and SAM.h (default version of SAM), which use ViT-L and ViT-H as the pre-trained, can attain more impressive results. Therefore, we encourage other researchers to explore the capacity of other SAM versions in this task. In addition, since our decoder is extremely simple, it can be studied to design a more complex one in order to enhance the performance of the model.

Acknowledgement

Dinh-Hieu Hoang was funded by Vingroup Joint Stock Company and supported by the Domestic Master/ PhD Scholarship Programme of Vingroup Innovation Foundation (VINIF), Vingroup Big Data Institute (VINBIG-DATA), code VINIF.2022.ThS.JVN.04. Nhat-Tan Bui and Ngan Le are sponsored by the National Science Foundation (NSF) under Award No OIA-1946391 RII Track-1, NSF 1920920 RII Track 2 FEC, NSF 2223793 EFRI BRAID, NSF 2119691 AI SUSTAIN, NSF 2236302, NIH 1R01CA277739-01. Minh-Triet Tran is sponsored by Vietnam National University Ho Chi Minh City (VNU-HCM) under grant number DS2020-42-01.

Table 5. Ablation study of the skip connection in our decoder. We report our results in the ACDC and Synapse datasets.

Settings	RV	LV	MYO	Average
w/o skip connection	88.46	94.41	86.32	89.73
w skip connection	89.44	94.67	87.12	90.41

(a) Ablation study in ACDC dataset.

Settings	Spl	RKid	LKid	Gal	Liv	Sto	Aor	Pan	HD↓	DSC↑
w/o skip connection	85.26	84.68	85.20	50.55	94.98	75.07	90.10	68.83	25.87	79.33
w skip connection	84.29	85.64	86.31	49.81	95.42	76.11	89.57	69.32	17.87	79.56

(b) Ablation study in Synapse dataset.

References

- [1] Reza Azad, Moein Heidari, Moein Shariatnia, Ehsan Khodapanah Aghdam, Sanaz Karimijafarbigloo, Ehsan Adeli, and Dorit Merhof. TransDeepLab: Convolution-Free Transformer-based DeepLab v3+ for Medical Image Segmentation. In *PRIME*, 2022. 2, 6
- [2] Olivier Bernard, Alain Lalande, Clement Zotti, Frederick Cervenansky, Xin Yang, Pheng-Ann Heng, Irem Cetin, Karim Lekadir, Oscar Camara, Miguel Angel Gonzalez Ballester, Gerard Sanroma, Sandy Napel, Steffen Petersen, Georgios Tziritas, Elias Grinias, Mahendra Khened, Varghese Alex Kollerathu, Ganapathy Krishnamurthi, Marc-Michel Rohé, Xavier Pennec, Maxime Sermesant, Fabian Isensee, Paul Jäger, Klaus H. Maier-Hein, Peter M. Full, Ivo Wolf, Sandy Engelhardt, Christian F. Baumgartner, Lisa M. Koch, Jelmer M. Wolterink, Ivana Išgum, Yeonggul Jang, Yoonmi Hong, Jay Patravali, Shubham Jain, Olivier Humbert, and Pierre-Marc Jodoin. Deep learning techniques for automatic mri cardiac multi-structures segmentation and diagnosis: Is the problem solved? *IEEE Transactions on Medical Imaging*, 2018. 2, 5
- [3] Sijing Cai, Yunxian Tian, Harvey Lui, Haishan Zeng, Yi Wu, and Guannan Chen. Dense-UNet: a novel multiphoton in vivo cellular image segmentation model based on a convolutional neural network. *Quantitative Imaging in Medicine and Surgery*, 10, 2020. 2
- [4] Hu Cao, Yueyue Wang, Joy Chen, Dongsheng Jiang, Xiaopeng Zhang, Qi Tian, and Manning Wang. Swin-Unet: Unet-like Pure Transformer for Medical Image Segmentation. In *ECCVW*, 2022. 1, 2, 6
- [5] journal=arXiv preprint arXiv:2102.04306 Chen, Jieneng and Lu, Yongyi and Yu, Qihang and Luo, Xiangde and Adeli, Ehsan and Wang, Yan and Lu, Le and Yuille, Alan L., and Zhou, Yuyin. TransUNet: Transformers Make Strong Encoders for Medical Image Segmentation. 2021. 1, 2, 6, 7
- [6] Jacob Devlin, Ming-Wei Chang, Kenton Lee, and Kristina Toutanova. BERT: Pre-training of Deep Bidirectional Transformers for Language Understanding. In *NAACL*, 2019. 2
- [7] Alexey Dosovitskiy, Lucas Beyer, Alexander Kolesnikov, Dirk Weissenborn, Xiaohua Zhai, Thomas Unterthiner, Mostafa Dehghani, Matthias Minderer, Georg Heigold, Sylvain Gelly, et al. An image is worth 16x16 words: Transformers for image recognition at scale. *arXiv preprint arXiv:2010.11929*, 2020. 1, 2, 4
- [8] Ali Hatamizadeh, Vishwesh Nath, Yucheng Tang, Dong Yang, Holger Roth, and Daguang Xu. Swin UNETR: Swin Transformers for Semantic Segmentation of Brain Tumors in MRI Images. *arXiv preprint arXiv:2201.01266*, 2022. 2, 7
- [9] A. Hatamizadeh, Y. Tang, V. Nath, D. Yang, A. Myronenko, B. Landman, H. R. Roth, and D. Xu. UNETR: Transformers for 3D Medical Image Segmentation. In *WACV*, 2022. 1, 2, 5, 6, 7
- [10] Kaiming He, Xiangyu Zhang, Shaoqing Ren, and Jian Sun. Deep Residual Learning for Image Recognition. In *CVPR*, 2016. 4
- [11] Moein Heidari, Amirhossein Kazerooni, Milad Soltany, Reza Azad, Ehsan Khodapanah Aghdam, Julien Cohen-Adad, and Dorit Merhof. HiFormer: Hierarchical multi-scale representations using transformers for medical image segmentation. In *WACV*, 2023. 2, 6
- [12] Edward J Hu, yelong shen, Phillip Wallis, Zeyuan Allen-Zhu, Yuanzhi Li, Shean Wang, Lu Wang, and Weizhu Chen. LoRA: Low-Rank Adaptation of Large Language Models. In *ICLR*, 2022. 3
- [13] Xiaohong Huang, Zhifang Deng, Dandan Li, and Xueguang Yuan. MISSFormer: An Effective Medical Image Segmentation Transformer. *arXiv preprint arXiv:2109.07162*, 2021. 1, 2, 6
- [14] Fabian Isensee, Paul Jaeger, Simon Kohl, Jens Petersen, and Klaus Maier-Hein. nnU-Net: a self-configuring method for deep learning-based biomedical image segmentation. *Nature Methods*, 18, 2021. 2, 6, 7
- [15] Debesh Jha, Pia H Smedsrud, Michael A Riegler, Dag Johansen, Thomas De Lange, Pål Halvorsen, and Håvard D Johansen. ResUNet++: An Advanced Architecture for Medical Image Segmentation. In *ISM*, 2019. 2
- [16] Davood Karimi and Septimiu E. Salcudean. Reducing the Hausdorff Distance in Medical Image Segmentation With Convolutional Neural Networks. *TMI*, 39, 2020. 6
- [17] Alexander Kirillov, Eric Mintun, Nikhila Ravi, Hanzi Mao, Chloe Rolland, Laura Gustafson, Tete Xiao, Spencer Whitehead, Alexander C. Berg, Wan-Yen Lo, Piotr Dollár, and Ross Girshick. Segment Anything. *arXiv:2304.02643*, 2023. 2, 3
- [18] Bennett Landman, Zhoubing Xu, J Igelsias, Martin Styner, T Langerak, and Arno Klein. Multi-Atlas Labeling Beyond the Cranial Vault - Workshop and Challenge. In *MICCAI Multi-*

Atlas Labeling Beyond Cranial Vault—Workshop Challenge, 2015. [2](#), [5](#)

- [19] Ze Liu, Yutong Lin, Yue Cao, Han Hu, Yixuan Wei, Zheng Zhang, Stephen Lin, and Baining Guo. Swin Transformer: Hierarchical Vision Transformer using Shifted Windows. In *ICCV*, 2021. [2](#)
- [20] Jun Ma, Yuting He, Feifei Li, Lin Han, Chenyu You, and Bo Wang. Segment anything in medical images, 2023. [3](#)
- [21] Xuebin Qin, Zichen Zhang, Chenyang Huang, Masood Dehghan, Osmar R. Zaiane, and Martin Jagersand. U2-Net: Going deeper with nested U-structure for salient object detection. *Pattern Recognition*, 106, 2020. [2](#)
- [22] Aditya Ramesh, Mikhail Pavlov, Gabriel Goh, Scott Gray, Chelsea Voss, Alec Radford, Mark Chen, and Ilya Sutskever. Zero-Shot Text-to-Image Generation. In *ICML*, 2021. [2](#)
- [23] Olaf Ronneberger, Philipp Fischer, and Thomas Brox. U-Net: Convolutional Networks for Biomedical Image Segmentation. In *MICCAI*, 2015. [1](#), [2](#)
- [24] Abdelrahman Shaker, Muhammad Maaz, Hanoona Rasheed, Salman Khan, Ming-Hsuan Yang, and Fahad Shahbaz Khan. UNETR++: Delving into Efficient and Accurate 3D Medical Image Segmentation. *arXiv:2212.04497*, 2022. [2](#), [5](#), [6](#), [7](#)
- [25] Amber L. Simpson, Michela Antonelli, Spyridon Bakas, Michel Bilello, Keyvan Farahani, Bram van Ginneken, Annette Kopp-Schneider, Bennett A. Landman, Geert Litjens, Bjoern Menze, Olaf Ronneberger, Ronald M. Summers, Patrick Bilic, Patrick F. Christ, Richard K. G. Do, Marc Gollub, Jennifer Golia-Pernicka, Stephan H. Heckers, William R. Jarnagin, Maureen K. McHugo, Sandy Napel, Eugene Vorontsov, Lena Maier-Hein, and M. Jorge Cardoso. A large annotated medical image dataset for the development and evaluation of segmentation algorithms. *arXiv preprint arXiv:1902.09063*, 2019. [2](#), [5](#)
- [26] Hugo Touvron, Thibaut Lavril, Gautier Izacard, Xavier Martinet, Marie-Anne Lachaux, Timothée Lacroix, Baptiste Rozière, Naman Goyal, Eric Hambro, Faisal Azhar, Aurelien Rodriguez, Armand Joulin, Edouard Grave, and Guillaume Lample. LLaMA: Open and Efficient Foundation Language Models. *arXiv:2302.13971*, 2023. [2](#)
- [27] Ashish Vaswani, Noam Shazeer, Niki Parmar, Jakob Uszkoreit, Llion Jones, Aidan N Gomez, Łukasz Kaiser, and Illia Polosukhin. Attention is All you Need. In *NIPS*, 2017. [2](#)
- [28] Xinlong Wang, Xiaosong Zhang, Yue Cao, Wen Wang, Chunhua Shen, and Tiejun Huang. SegGPT: Segmenting Everything In Context. *arXiv:2304.03284*, 2023. [2](#)
- [29] Lauren H. Williams and Trafton Drew. What do we know about volumetric medical image interpretation?: a review of the basic science and medical image perception literatures. *Cognitive Research: Principles and Implications*, 4, 2019. [1](#)
- [30] Kaidong Zhang and Dong Liu. Customized Segment Anything Model for Medical Image Segmentation. *arXiv preprint arXiv:2304.13785*, 2023. [3](#), [6](#), [7](#)
- [31] Hong-Yu Zhou, Jiansen Guo, Zhang Yinghao, Lequan Yu, Liansheng Wang, and Yizhou Yu. nnFormer: Interleaved Transformer for Volumetric Segmentation. *arXiv preprint arXiv:2109.03201*, 2021. [2](#), [4](#), [5](#), [6](#), [7](#)
- [32] Zongwei Zhou, Md Mahfuzur Rahman Siddiquee, Nima Tajbakhsh, and Jianming Liang. UNet++: Redesigning skip

connections to exploit multiscale features in image segmentation. *TMI*, pages 1856–1867, 2020. [2](#)